Technology Transfer Plan

LuNaMaps Project

NASA Goddard Space Flight Center

August 30, 2024
Version 1.1

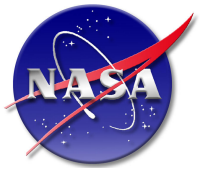

National Aeronautics and Space Administration

Technology Transfer Plan

for the

Lunar Navigation Maps (LuNaMaps) Project

Prepared by:

GSFC: Carolina Restrepo, Noah Petro, Mike Barker, Erwan Mazarico, Stephen Scheidt, Jacob Richardson, Stefano Bertone, Chris Gnam, Andrew Liounis
ARC: Ross Beyer
JPL:Yang Cheng, Adnan Ansar, Cecilia Mauceri, Yumi Iwashita, Zachary Morgan

Approved By:

Andrew Liounis
LuNaMaps Project Manager
Goddard Space Flight Center

Summary

The main contribution of this project is the combined knowledge of terrain relative navigation experts and lunar scientists who are familiar with both the lunar orbital imagery and the instruments that collected the data as well as how a TRN system utilizes map data. This knowledge comes in the form of published technical papers, benchmark map data sets, and software tools that can help others automate the process of creating the necessary maps for their own landing sites in the future. This document represents the project's plans to share all the lessons learned, processes developed, and applicable software tools with the public.

TABLE OF CONTENTS

1 Introduction

The main contribution of this project is the combined knowledge of terrain relative navigation experts and lunar scientists who are familiar with both the lunar orbital imagery and the instruments that collected the data as well as how a TRN system utilizes map data. This knowledge comes in the form of published technical papers, benchmark map data sets, and software tools that can help others automate the process of creating the necessary maps for their own landing sites in the future. This document represents the project's plans to share all the lessons learned, processes developed, and applicable software tools with the public.

There are 3 NASA centers participating in the project, and each center has its own native tools that have been modified or adapted for the purpose of generating lunar map products. The JPL tools are based on work performed for the Mars missions. Goddard has developed new tools for the purpose of cleaning up map errors and artifacts as well as improving map resolution. Additionally, Goddard is making use of TRN tools that were originally developed for small body and asteroid missions and have been adapted to be able to load large lunar map sets and run lunar landing scenarios. Ames has an open source tool called the Ames Stereo Pipeline (ASP), however running this tool requires a high level of expertise.

Fig. 1 captures the need for multiple map products throughout a lunar landing scenario.

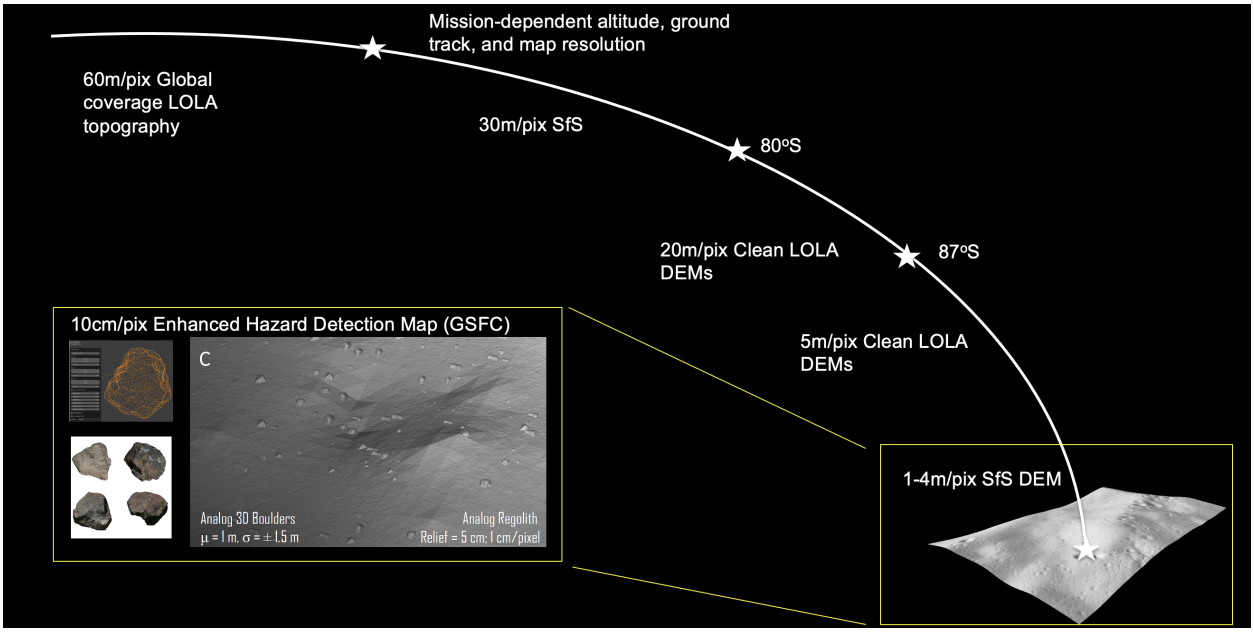

Figure 1: Maps for Landing with both TRN and Hazard Detection Onboard

Topography data is available for the entire Moon at 60 meter/pixel (m/pix) resolution. Our assumption is that TRN systems will need better resolution than 60 m/pix for specific areas of the Moon along the ground track of a given trajectory. Therefore, to determine the best way to obtain these maps, we used an example trajectory that lands on the Connecting Ridge of Shackleton Crater.[1] We made Shape from Shading (SfS) maps for the areas which would be visible by a TRN camera (nadir pointing) with a ground sample distance of 30 m/pix below 20 km altitude, corresponding to a lunar latitude of 80° South. Between 80° and 87° South, the LOLA topography is now 20 m/pix and between 87° and 90° South is 5 m/pix, which should

[1] An area of interest as demonstrated by being the target for the Intuitive Machines Nova-C lander. https://www.nasa.gov/missions/artemis/clps/nasa-intuitive-machines-announce-landing-site-location-for-lunar-drill/

be sufficient for TRN. These maps are all based on orbital imagery and the uncertainties in the data are now well understood due to work by the project. We additionally considered the Apollo 16 landing site and generated high resolution SfS maps of this area at 1 m/pix.

Separately, synthetically enhanced digital elevation models (DEMs) are generated by taking a much smaller area around the landing site, in this case 200x200m, of the 1 m/pix SfS DEM, and interpolating the data to make that base terrain 10 cm/pix. Once the base (real) terrain is at a resolution of 10 cm/pix, synthetically generated realistic lunar rocks are added to the terrain resulting in a new enhanced DEM that contains lunar lander scale hazards. Various DEMs can be generated with the base terrain by using different numbers for the rock and crater size and abundance distributions.

The following sections describe the processes that have been developed to generate the map products described as well as some of the scripts that the various team members have developed to date. Some of these scripts will become user-friendly software tools that can be shared with the public. However, some scripts will be described in conference or journal papers rather than in the form of a software tool due to the risks of having inexperienced users running a tool without the necessary geology or navigation background producing the wrong results.

2 Shape from Shading DEMs for a Lunar Landing Ground track

The goal is to generate terrain maps at resolutions close to the ground sample distance of a sample onboard TRN camera. The resolutions generated for our use case are shown in Fig. 2.

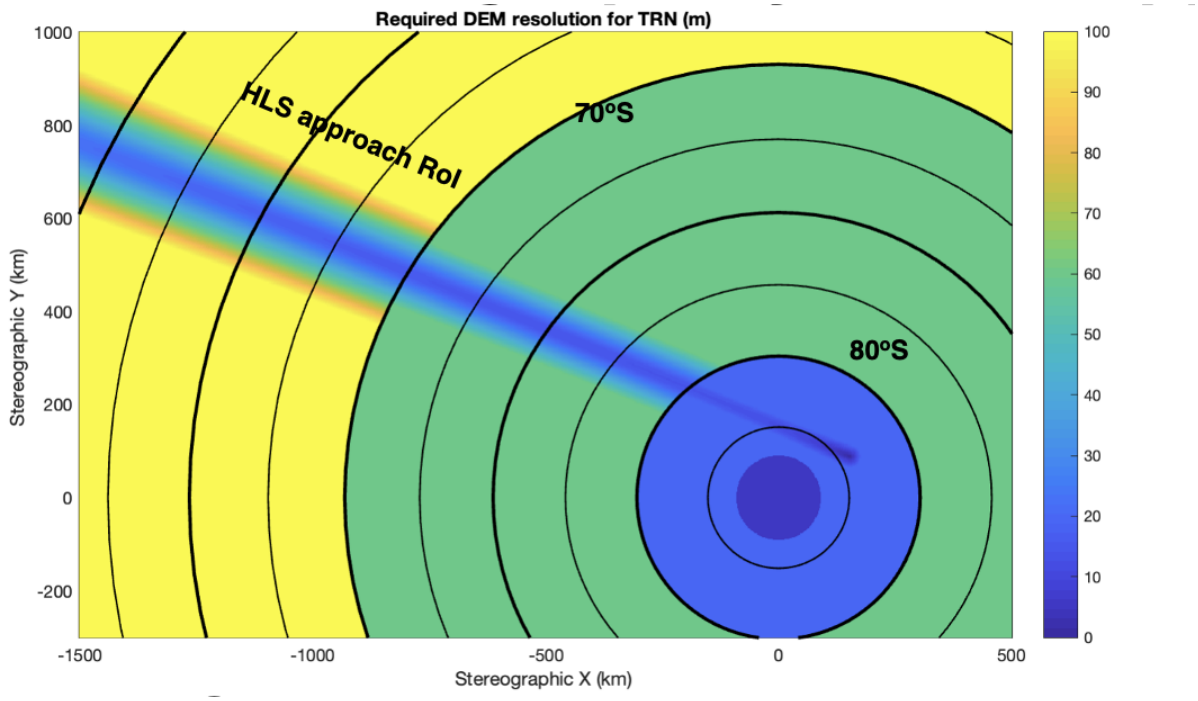

Figure 2: DEMs for South Pole Landing Approach

Team members from Goddard's Planetary Geology, Geophysics and Geochem Laboratory used the Ames Stereo Pipeline and a combination of various python scripts for:

- Locating the lunar terrain visible from an onboard, nadir-pointed 45° deg Field-of-View TRN camera

- Collecting the available LROC NAC images for the regions of interest
- Obtaining the LOLA topographic maps for the regions of interested
- Tiling up the path into smaller pieces of terrain (10x10km)
- Performing image bundle adjustments
- Aligning images to topography
- Performing coordinate transformations and shifts between data sets
- Comparing SfS DEMs to LOLA DEMs
- Comparing rendered DEM images to NAC images

Technology Transfer

The team has shared detailed information on the process, along with the scripts used, and the resulting DEM products in a web article publicly accessible at `https://pgda.gsfc.nasa.gov/products/92`.

3 Clean LOLA DEMs

Michael Barker at Goddard developed a process to clean LOLA topographical data at different resolutions. He had already developed the process before this project started and had mapped a few distinct sites near the south pole. When LuNaMaps started, we set the goal of covering the entire area between 87°–90° deg South at 5 m/pix resolution, and the area between 80°–87° South at 20 m/pix.

This work has been completed and documented in technical papers and published on publicly accessible websites. The software that was developed to clean the LOLA topography data will not be shared because it is specific to LOLA and 100% of the resulting data has been made public, so there will not be a need for anyone else to re-generate it. The technical papers explain the process fully and all the steps that were taken to validate the data along with information on uncertainty values and where they come from.

Technology Transfer

The process of generating the high resolution DEMs has been published in [1] and [2]. The resulting products can be found at `https://pgda.gsfc.nasa.gov/products/81` for the 87°–90° region and `https://pgda.gsfc.nasa.gov/products/90` for the 80°–87° region.

4 Shape from Shading DEM of Apollo 16 Landing Site

The data products for the 12 $\times$ 28 km area around the Apollo 16 landing site were generated using open source software tools at NASA Ames. The nuances, caveats, and lessons learned will be shared/published along with the data set itself once the team at Ames submits their paper on the data set. Currently, our team has been working with a pre-release version of the to-be-released data set for use in our work plans and the development of analysis tools.

Since the Apollo 16 site is an equatorial location and not polar, the improved maps from Section 3 could not be used as the terrain reference. Instead, we used the 60 m/pix SLDEM 2015 product [3], and we used the Geospatial Data Abstraction Library (GDAL [4]) to interpolate the source maps to 1 m/pix. The hillshade maps were also created via GDAL [4]. The Integrated Software for Imagers and Spectrometers (ISIS, v 5.0.1, [5]) was used for initial processing of the Lunar Reconnaissance Orbiter Camera (LROC) images. All the other data products in this package were created with the NASA Ames Stereo Pipeline (ASP, v 3.0.0, [6]), specifically using the techniques described Ref. [7] for creation of the SfS terrain model.

These data products are absolutely controlled map products, because they are bundle-adjusted and rigorously tied to the underlying SLDEM product. The SLDEM and SfS-DEM products are orthonormic heights relative to the reference lunar radius of 1,737,400 m.

The LROC NAC maps and the maximally-lit mosaic are orthorectified and have had their pixels projected onto the SfS terrain model. Pixel values in these data products were sourced from images that were radiometrically calibrated via ISIS [3] and are thus in units of irradiance/flux (I/F).

The data products included in this package are included in Table 1.

Table 1: Description of files in the dataset

Filename	**Description**
`LROC_NAC_maps/M*map*.tif`	LROC NAC images orthorectified to the SfS DEM. These are 32-bit grayscale GeoTIFF files.
`LROC_NAC_maps/resolution.tif`	A mosaic which indicates the resolution in m/pix of the best resolution LROC NAC image that covers a particular pixel.
`A16-sldem.tif`	A section of the 60 m/pix SLDEM terrain cropped to the Apollo 16 area and over sampled to 1 m/pix.
`A16-sfs-dem.tif`	SfS DEM as a GeoTIFF with 32-bit pixels indicating the elevation with respect to the lunar radius of 1,737,400 m at 1 m/pix.
`A16-sfs-dem-hs.tif`	The above SfS DEM's hillshade.
`A16-sfs-height-error.tif`	A height uncertainty product derived from creating simulated images by taking the SfS DEM and illuminating it in a manner similar to each source image. Pixel values in the height-error map are the maximum height perturbation at each pixel, in meters, that results in one of the simulated images (which correspond to each original image) diverging from the corresponding original image by more than twice the difference between the unperturbed simulated image and the original image. This is a 32-bit GeoTIFF. Areas that were not illuminated by any source image have their pixels set to the no-data value.

This Apollo 16 lander is located at approximately 15.5011° E, 8.9734° S and the bounding box of this terrain model is specified by the coordinates in Table 2.

Table 2: Apollo 16 Area Bounding Box

	Longitude / Latitude (deg)
Upper Left	15.15251 E, 8.64602 S
Lower Left	15.15161 E, 9.57548 S
Upper Right	15.54808 E, 8.64617 S
Lower Right	15.54821 E, 9.57565 S

Technology Transfer

The SfS DEMs generated by the team will be part of the publicly released benchmark TRN data sets. We plan to release them to the Planetary Data System (PDS) Cartography and Imaging Sciences Node Annex. These use the Ames Stereo Pipeline [6], and it is already an open source software. The lessons learned by the team at Ames will be included in the release package with all the images and map products so that others can generate similar results for other locations on the lunar surface. We are also working on a paper in the Planetary Sciences Journal describing this work.

5 Synthetic High Resolution Surface Features for Hazard Detection DEMs

There is a need to model synthetic surface features for the lunar surface (small rocks and craters) that are smaller than those which can be seen from orbit but large enough to be hazardous to a lander for the purposes of testing hazard detection and avoidance (HDA) algorithms as well as simulating surface traversals for rovers and astronauts. In the LuNaMaps project we have pursued development of three related but distinct capabilities to cover a wide range of needs for synthetic DEM enhancement. These include the rocky surface generator software, the synthterrain software, and the Synthetic Lunar Terrains software. We briefly describe each tool and its release in the following subsections.

5.1 Rocky Surface Generator

The LuNaMaps Rocky Surface Generator contains a rock library and a suite of scripts that use this library to insert cm-scale resolution rocks as well as synthetic craters into an existing DEM to output an overall synthetically enhanced DEM. The new DEM contains lunar-like rocks buried and distributed according to the statistics of past landing sites as well as user-input rock parameters and statistics making it a very practical and user-friendly tool to generate lunar terrains for simulating on-ground surface operations that require realistic maps. It additionally contains craters with a wide range of morphologies according to the current best estimate crater distributions.

5.1.1 Rock Library

The Goddard Instrument Field Team collected data in Iceland (Fig. 3–4) in 2021 and some rocks from the drone stereo-imagery were used for this project, as well as rocks from other locations that field geologists considered lunar-like to add enough variety to the rock library. The rocks were mirrored about the burial plane to make them full rocks (Fig. 5) so they can be scaled, buried, and rotated by the software.

Technology Transfer

The rock library model rocks will be made public at either the PDS Annex or the USGS Archive for analog materials. We will include a description of the rocks in the library and pointers to the rocky surface generator software.

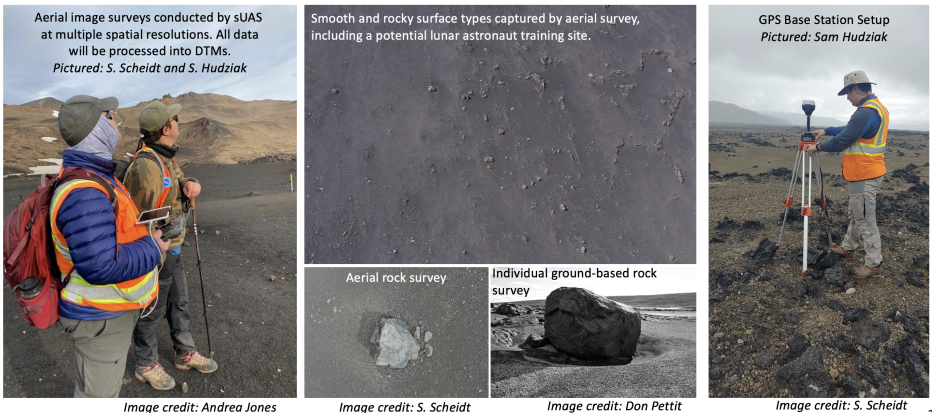

Figure 3: Field Data Collection in Iceland

- From: **Scheidt SP**, JA Richardson, MK Barker, NE Petro, CI Restrepo, E Mazarico, L Kerber (2021). Application of Earth-analog sites for lunar simulated digital terrain models. Joint 2021 NASA Exploration Science Forum and European Lunar Symposium 2021, July 20-23.

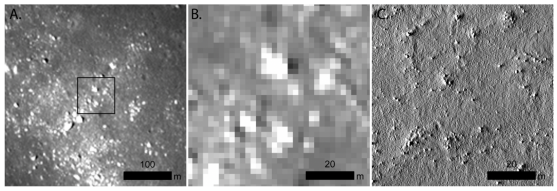

A) Impact crater ejecta (LROC NAC image M126710873R). B) Inset view of ejecta. C) Boulder field on a sand sheet in northern Iceland near the Askja and Holuhraun eruptions. Hillshade of 5 cm/pixel resolution sUAS-generated DEM the same scale.

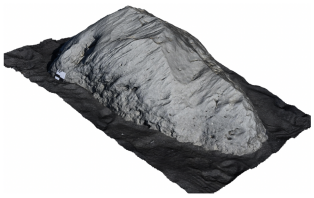

Example of a high-resolution basaltic rock model from the boulder field in northern Iceland shown above, rendered in 3D. The black and white scale bar against the rock is 10 cm.

Figure 4: Example rock from stereo-imagery

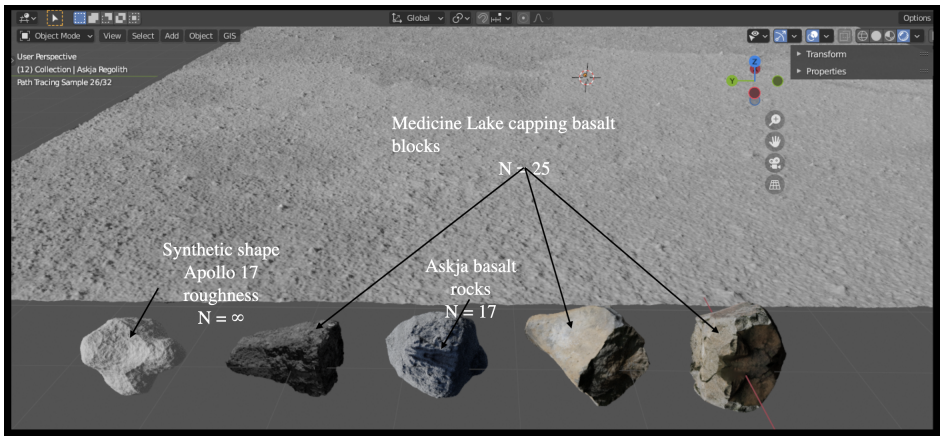

Figure 5: 3D Rock Assets, N = Rock Variations

5.1.2 Rocky Surface Generator Software

The software takes in a 'base DEM', in this case the SfS DEM described in Section 4, and interpolates the data to achieve cm-scale resolution before adding the surface features. In addition to the base DEM, the code takes in the rock size distribution models from [8] in the form of a power law ($N = kD^r$) fit to NAC or in situ observations (or both) from the CE-3, Apollo 11, Apollo 16, and Surveyor I, III, VI, and VII locations. The rock burial depth is based on [9]. The average burial depth used is 50% ± 20% and the rock locations are randomly distributed.

Fig. 6 is an example output plot of a rock distribution for an output DEM from the software, and Fig. 7 shows the various pre-set rock distribution options and their locations that are listed in the code for users to select from. Fig. 8 is an example output DEM.

Prior to adding rocks to the synthetic lunar surface, a population of craters is added that includes craters below detectable limits in 1 meter SfS DEMs. The synthetic crater generation code (written in Python) takes in the crater size frequency distribution (CSFD) model shown in Fig. 9 in the form of a power law for small sized craters (N = 0.039811D-1.83) [10]. The shape of fresh and degraded small craters is well studied, but is frequently characterized by crater age, as shown in Fig. 10 [11, 12, 13, 14, 15]. Our current code creates a set of fresh craters according to a CSFD, and then adds craters, progressively from degraded or modified (i.e., older) to fresh (i.e., younger) onto a flat base plane or a base DEM. Each new crater impact takes into account the previous topography so that any coincident or overlapping crater will alter the topography of the underlying crater and terrain. Most small craters are flat-bottomed or concentric [14], and therefore modeling central uplift is not necessary. Degradation occurs due to mass wasting and land surface diffusion, and can be modeled using diffusivity over time, $\kappa\tau$ [11, 12]. Our code utilizes a frequency distribution of the maximum crater wall slope, which in our initial work utilizes the Design Specification for Natural Environments (DSNE) [15], also shown here in Table 3. Modification of crater shape is achieved by incorporating a land surface diffusion model for crater erosion, which is time-step dependent and a key feature of this code implementation. Each crater profile is modified by the diffusion model until reaching a specified slope in the frequency distribution. Crater age is not assigned due to the uncertainties of real crater ages. For a crater size frequency distribution, the user can specify a size range. Specifying 0.4 to 25 m diameter will result in 6000 craters in a 100 m × 100 m area. The code user has the option for producing a flat plane with a crater population, as shown in Fig. 11, and can be added to the base DEM by raster addition, or the craters can be populated directly on the base DEM.

Technology Transfer

We plan to share this software through the University of Maryland.

5.2 synthterrain

The synthterrain software is a tool capable of generating statistically correct crater and rock size frequency distributions at varying length scales. The tool enables a user to generate rock distributions which can be combined with a rock library to augment a DEM with additional rocks, though it currently does not directly add rocks to an existing DEM. It also generates crater distributions with varying morphologies and is able to add these craters to existing DEMs through carving. It is written in python.

The tool provides an array of crater distributions from the unpublished VIPER Environmental Spec, the Trask distribution [10], the Neukum coefficient distribution [16], the Neukum production function distribution [16], the Grun function distribution [17], and custom blends of the Neukum and Grun functions. It also

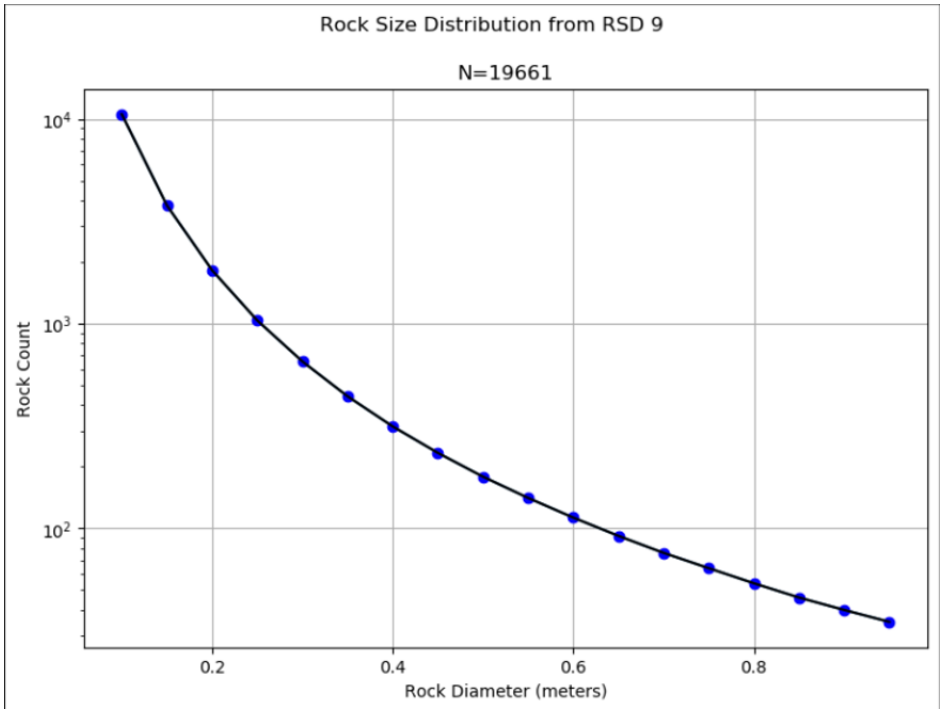

Figure 6: Example Rock Size Distribution Statistics

```
############## ROCK SIZE DISTRIBUTION ###################
# For rock size-frequency distributions explanation, see:
# Li, B., Ling, Z., Zhang, J., & Chen, J. (2017). Rock size-frequency distributi
# landing sites based on remote sensing and in-situ imagery. Planetary and Space

#After Table 6 in Li et al., (2017):
print(" ")
print("Landing site                        Data sources  k        r     R_sq")
print("1.  CE-3                            In-situ       0.00275  -1.86 0.989")
print("2.  CE-3                            NAC           0.00528  -2.63 0.982")
print("3.  Apollo11                        In-situ       0.00380  -2.24 0.941")
print("4.  Apollo11                        NAC           0.00250  -3.81 0.941")
print("5.  Apollo 16 stations 4, 5 and 6   NAC + In-situ 0.00022  -4.20 0.965")
print("6.  Surveyor I                      NAC + In-situ 0.00114  -2.23 0.963")
print("7.  Surveyor III                    NAC + In-situ 0.00060  -2.58 0.971")
print("8.  Surveyor VI                     NAC + In-situ 0.00016  -2.77 0.965")
print("9.  Surveyor VII                    NAC + In-situ 0.00311  -2.53 0.978")
print("10. Manual entry                    User specified")
print("11. Synthetic Normal Distribution   Statistical")
print(" ")
Q2 = input("Select rock size distribution parameters of the function N = kD^r. E
```

Figure 7: Varying Rock Size and Abundance Options.

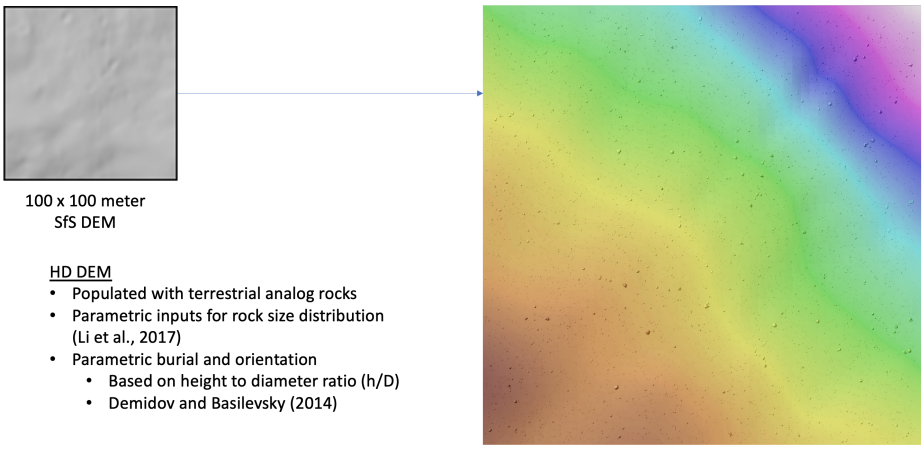

Figure 8: Example DEM with added rocks.

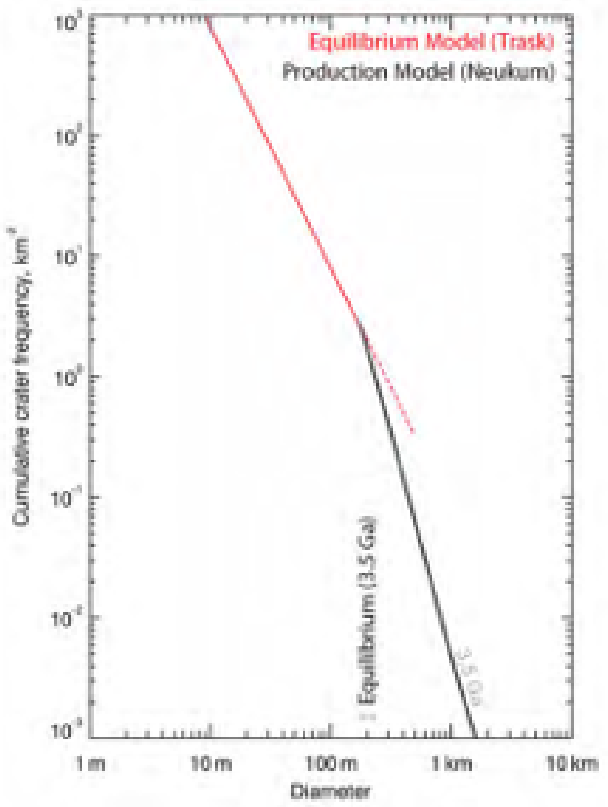

Figure 9: The crater size frequency distribution according to [10].

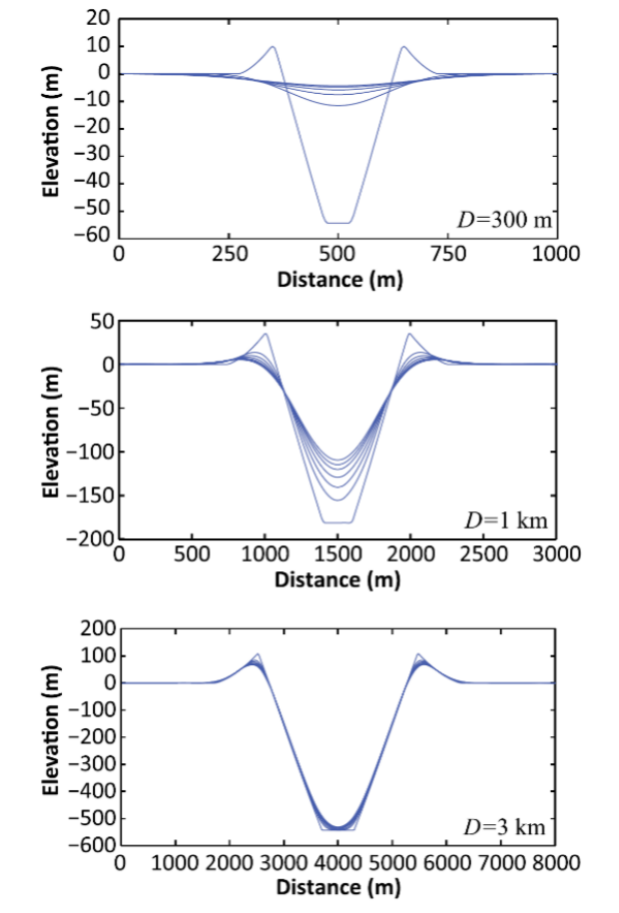

Figure 10: Crater profiles showing progressive degradation in [11, 12].

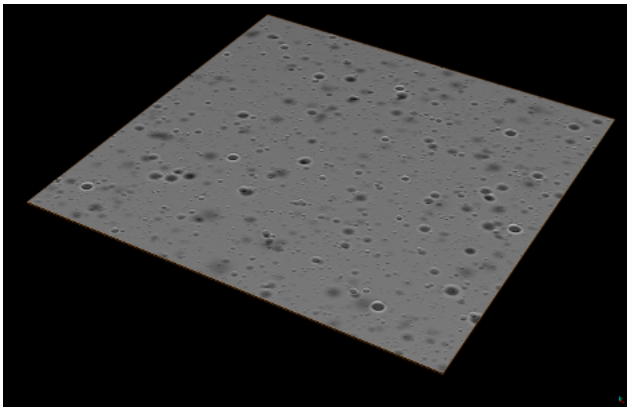

Figure 11: Synthetic crater population according to a maximum slope distribution specified by [15].

Table 3: Slope distribution and characteristics based on [15]

	Freshest Craters		Degraded Craters		
Fraction of population	0.5%	2.5%	17%	30%	50%
Crater Characteristics	Very steep slopes, pronounced blocks, ejecta, optically immature	Steep slopes, blocks common	Moderate slopes, most blocks on rim	Gentle slopes, rim mostly eroded	Very gentle slopes, no rim
Typical depth/diameter ratio	0.12-0.2+	0.12-0.2	0.1-0.15	0.07-0.1	<0.07
Max. Wall Slope	35°+	25-35°	15-25°	10-15°	<10°

provides an array of rock distributions from the unpublished VIPER Environmental Spec, and 2 unpublished internal distributions.

Examples of the outputs from synthterrain are available in Figs. 12 and 13.

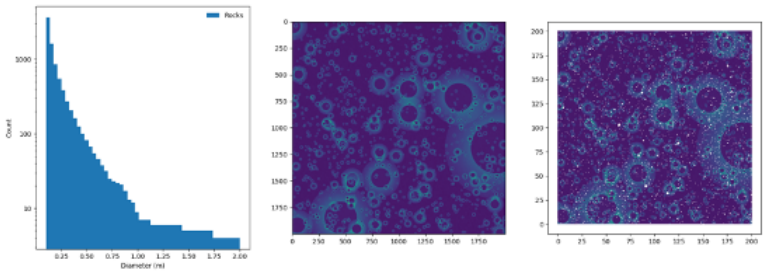

Figure 12: Example rock distribution from synthterrain.

Technology Transfer

An initial version of synthterrain has been completed and publicly released at `https://github.com/NeoGeographyToolkit/synthterrain`. We plan to continue to maintain the software and increase its capabilities.

5.3 Synthetic Lunar Terrains

The Synthetic Lunar Terrains (SLT) tool enables augmenting existing DEMs with synthetic craters and rocks (from a rock library). The tool applies the latest distribution statistics for both craters and rocks to an existing DEM, enabling creation of realistic synthetic DEMs for testing purposes. The tool also supports rendering the synthetic terrain with realistic lighting in a range of scenarios. The rock library used currently consists of

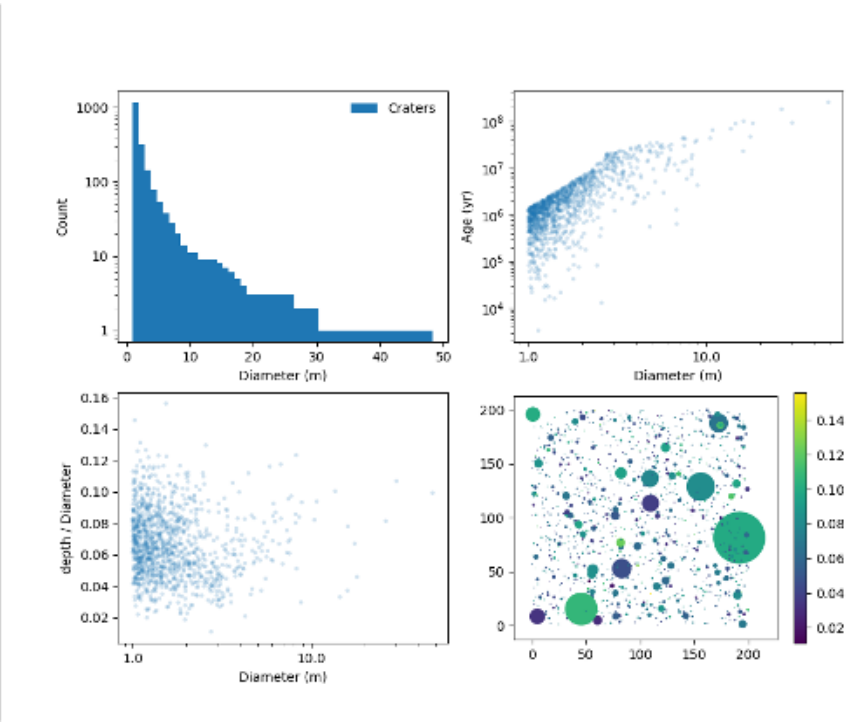

Figure 13: Example crater distribution from synthterrain.

scans of the Apollo rock collection [18] and synthetically generated rocks. An example of the DEM creation and visualization process is shown in Fig. 14.

Technology Transfer

The authors plan to release the SLT tool open source through JPL's GitHub (`https://ghitub.com/nasa-jpl`).

6 Map Validation Software Tools

JPL has focused on developing tools and methods for validating TRN maps. In this context, map validation and verification is the processes of ensuring the accuracy and reliability of maps for Lunar TRN. Fig. 15 shows the main types of errors that these tools seek to understand and mitigate as much as possible. Due to a lack of ground truth, our general approach will focus on reducing risk by (1) independent processing of data using separate workflows and tools and (2) cross validation using unrelated datasets and data from different sensor modalities.

We organize validation into two broad categories: (1) Low level data correction and preparation and (2) high level comparison of data products. The data correction step also factors into the process of map generation. These are described in more detail in the following subsections.

(a) Base DEM (b) Enhanced DEM (c) Rendered Enhanced DEM

Figure 14: Example DEM augmentation using SLT.

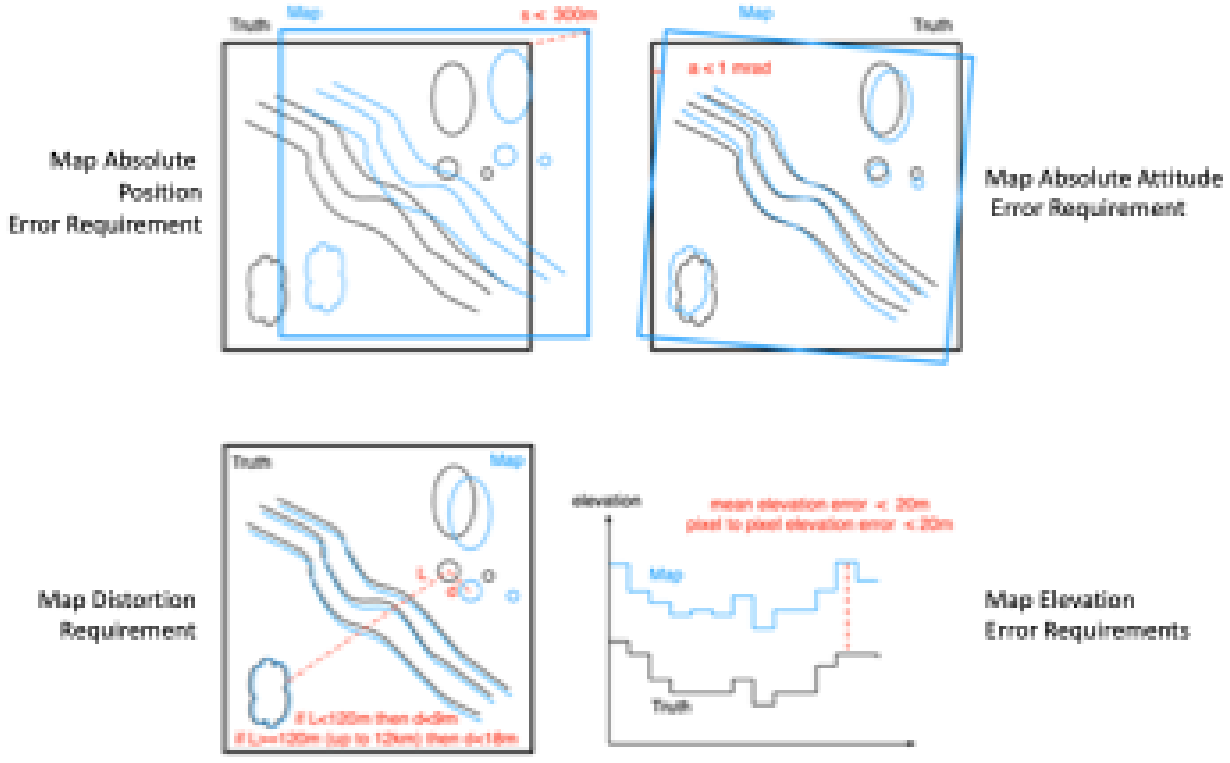

Figure 15: DEM Errors

Technology Transfer

The authors plan to release the DEM comparison/validation tools open source through JPL's GitHub (`https://ghitub.com/nasa-jpl`).

6.1 Low-level data correction and preparation

The key object is to align all data precisely into the same coordinate frame. Often, both the spacecraft orbit determination (OD) solution and pointing solution are not sufficiently accurate to natively align the input images to the pixel level. We perform this with respect to a locally defined Cartesian frame, which results in significant computational simplification. Since the mapping from this local Cartesian frame to a global Lunar body frame is a closed form transformation, there is no loss of generality in this approach.

The relationships between reference frames (Cartesian, TRN, Camera, Spacecraft) are not trivial and require careful data manipulation to ensure that the image pixels can be accurately represented in the TRN map. The methods developed at JPL go through this process meticulously and have been proven to eliminate a significant amount of error in the images. After image correction, the results can be compared to other map products. JPL has performed corrections to images from NAC as well as from the Kaguya Terrain Camera.

6.2 High level comparison of data products

Comparing the corrected images and maps using the tools for the low-level corrections to the NAC images and the Kaguya TC images requires one to collect all the relevant images via online databases. While the tools to find the NAC images are functional, the online interfaces are challenging when trying to find and download hundreds of NAC images. We have developed a multistep, semi-automated approach to downloading NAC images of interest.

6.2.1 Assessment of Shape from Shading DEM using NAC imagery

We selected a NAC image (M1111220875) at the DRM2 site for comparison to a SfS DEM generated by Ames. The SfS DEM was rendered with lighting conditions matching the NAC image (Fig. 16). These were then matched to each other on a per-pixel basis using dense correlation matching.

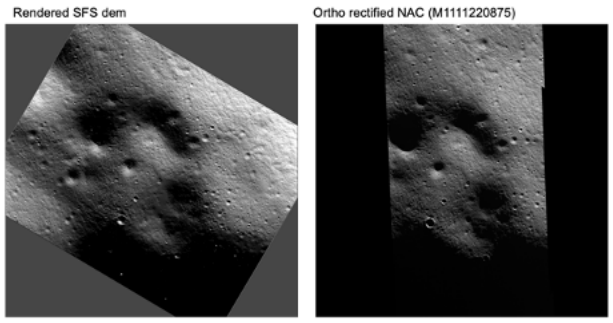

Figure 16: DEM Errors

A large shift (24 m in X and 48 m in Y) was observed between the two. This large bias is due to differences in OD and bundle adjustment applied to the data used for SfS. The systematic error can be ignored. More concerning was that the standard deviations between the products (3.6 m x 4.1 m) are much larger

than the 1 m resolution of the DEM. See Fig. 17. Further investigation revealed a series of discontinuities in the SfS DEM of 2 m in magnitude. The SfS product in question was not finalized, and Ames was aware of processing errors which since have been corrected. Nevertheless, this result points to the utility of this process for assessing DEMs.

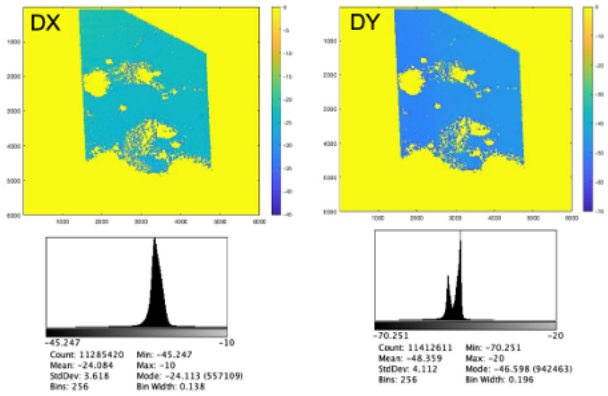

Figure 17: Large standard deviations in X and Y disparity maps between NAC and rendered SfS DEM reveal potential issues.

6.2.2 Assessment of LOLA native resolution using NAC imagery

The true resolution of a DEM may not match its advertised size. Instead, true spatial resolution refers to the size of the smallest feature that can be detected. Lunar TRN maps are likely to be rendered products from DEMs, so it is important that there be mechanism to evaluate resolution independent of meta-data. Fig. 18 shows a NAC image down sampled to 5 m/pix on the left and an image rendered from LOLA, notionally at 5 m/pix, on the right. The true resolution difference is apparent.

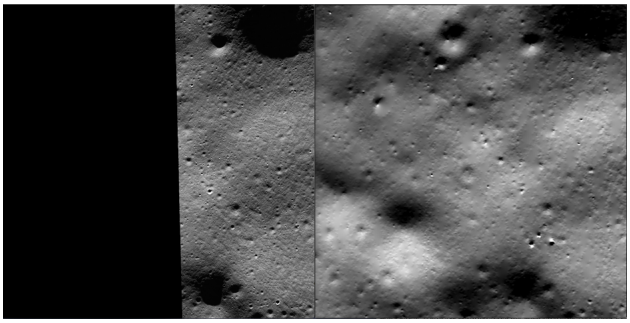

Figure 18: 5 m/pix NAC image on left. Render from 5 m/pix LOLA DEM on right. The left image has much higher resolution than the right

We present a simple method to indirectly assess native resolution by progressively down sampling NAC images, computing a correlation map to the original and assessing when this matches the correlation to the rendered LOLA DEM. Similar behavior will result from similar spatial frequency content.

Fig. 19 shows the same NAC image, progressively down sampled to 40 m/pix. Fig. 20 shows the correlation maps between the original NAC image at 5 m/pix, and its downgraded versions as well as the correlation map between the original NAC image and the rendered LOLA DEM. The behavior is consistent

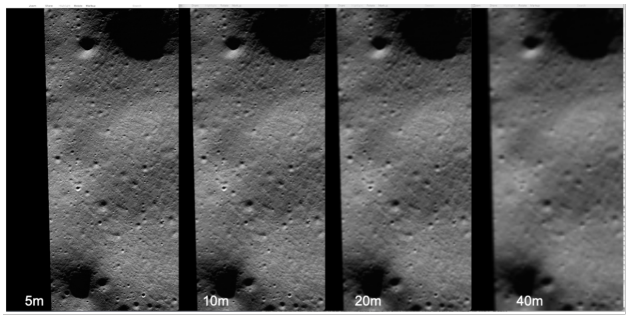

Figure 19: NAC image, progressively down sampled

with a native resolution for the LOLA DEM between the second and third down samplings, i.e. between 20 m/pix and 40 m/pix. While the LOLA team is aware that the 5 m posting in this case is not reflective of the true resolution, we believe a method to assess this independently has value in generating maps. The true resolution of an underlying DEM must factor into the error budget of a TRN algorithm.

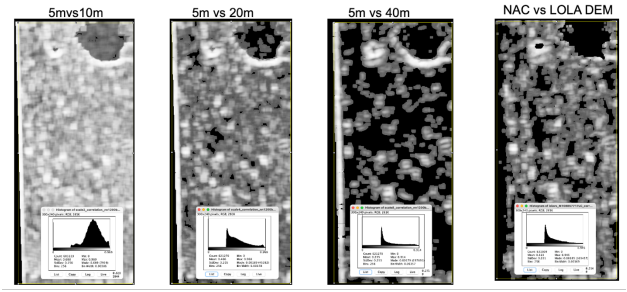

Figure 20: Correlation maps between original and downsampled NAC (first 3 images) and between Original NAC and rendered LOLA (last image). The match behavior indicates that the LOLA DEM has a resolution between 20 and 40 m/pix

6.2.3 Assessing Kaguya DEM Quality

The Kaguya Terrain Cameras have 10 m/pix image resolution and DEM resolutions that approach this. However, the DEMs downloaded directly from the JAXA website have artifacts that make them less suitable for use in validation. Fig. 21 shows the marked difference between Kaguya TC imagery on the left and renders from the JAXA produced DEMs. In light of this, JPL has developed its own process for generating Kaguya DEMs, which are used here for comparisons with the SfS DEMs.

To compare the Kaguya DEM to the LOLA DEM, both maps are projected into a common reference frame. Once they are in the same projection, they are compared using dense feature correlation methods. For the dense feature correspondence, we correlate the surface reflectance maps of the two DEMs. The Kaguya DEM has a surface reflectance map provided by the pixel values of the images from which it was created. For the LOLA DEM, we render a hillshade map and use it as a proxy for surface reflectance. The hillshade is rendered with the same sun angle as the time when the Kaguya images were captured. The dense feature correspondence calculates the most likely matching patch in the Kaguya map for each pixel in the LOLA map. It outputs the correlation score for each pixel, as well as, the patch offset. The patch offsets are visualized in the following figure. No significant distortion or relative image jitter is found between

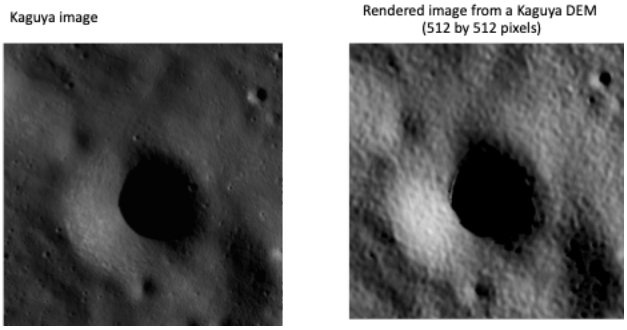

Figure 21: Comparison of Kaguya Terrain Camera image with a DEM generated from a JAXA produced DEM.

them. There is a small inconsistency in the edge pixels of Kaguya DEM, which is likely caused by residual, uncorrected camera model error. However, the error is smaller than one pixel. The standard deviations in X and Y disparity are on the order of 10 m, which is half the resolution of the LOLA DEM. This indicates that the Kaguya DEM and LOLA DEM have good agreement along the surface.

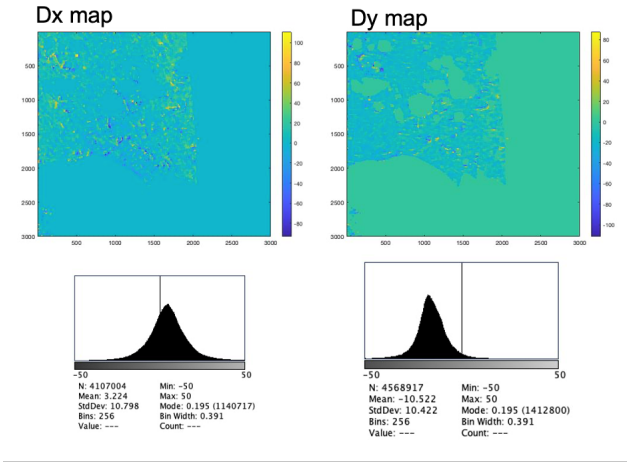

Figure 22: The X and Y disparity maps show good agreement between the LOLA and Kaguya DEMs

We also compared the elevation difference between LOLA and Kaguya DEMs as well as a SfS result at the same location. Means are near zero in all cases, and the standard deviation is less than 3 m in all cases. In particular, that between the SfS and Kaguya DEM is 1.4 m, which is well below the spatial resolution of the Kaguya DEM.

7 TRN Validation Pipeline

In addition to validation of map quality with respect to how well it matches the true surface, it is useful to examine map quality with respect to how well it supports terrain relative navigation. For motivation, consider a DEM that perfectly represents a planar surface. We can say that this DEM has extremely high quality with respect to how well it matches the true surface, it does so perfectly. However, this DEM will have extremely low quality for passive TRN (using a monocular camera) (though of course it could be used

for active TRN successfully generating altitude measurements). In order to enable users to evaluate how well a set of maps can support various TRN algorithms we have developed a TRN validation pipeline.

The TRN validation pipeline is outlined as follows:

1. Provide a nominal flight profile, "ground truth maps", and navigation maps.
2. Apply variations systematically to the time of day the flight profile is flown, the actual flight profile flown, the underlying "ground truth map", among others, potentially informed from the previously discussed map validation pipeline.
3. Simulate image and active ray tracing using the Vira ray tracer developed by this project.
4. Apply chosen TRN algorithms to the simulated data using either ground software (like the Goddard Image Analysis and Navigation Tool (GIANT) [19]), or actual representative flight software (FSW) implementations.
5. Feed the extracted TRN observables to a navigation filter (like Monte [20]) or actual representative flight software implementations (like GEONS [21]).
6. Repeat 2–5 for a defined range of variations
7. Provide results for verification and analysis.

Technology Transfer

This process will be described in an upcoming paper at the AIAA SciTech conference in January 2025. We will additionally publish the various components and scripts used for the process through the agency GitHub (`https://github.com/nasa`). Some components are already publicly available (either open source or US persons) including:

- GIANT `https://github.com/nasa/giant`
- MontePy `https://montepy.jpl.nasa.gov`
- GEONS `https://software.nasa.gov/software/GSC-14687-1`
- core Flight System (cFS) `https://github.com/nasa/cfs`

We expect to release the remaining scripts and tools, including Vira and representative flight software TRN applications in the cFS ecosystem [22], in early 2025.
We additionally are using this tool suite to generate parametric TRN models which can be used to predict TRN performance across a wide range of scenarios.

7.1 Vira

Vira is a ray tracing and rendering Application Programming Interface (API) built for engineering and scientific applications. While there are existing rendering APIs, many are optimized for artistic purposes such as for video games or visual effects, which while they can produce photorealistic results, lack the flexibility to directly tackle certain engineering problems. Other APIs, such as NASA's Goddard Image Analysis and Navigation Tool (GIANT) offer the flexibility engineers need but lack the efficiency of modern renderers and ray tracers. Vira aims to provide a high-level API that utilizes modern graphics programming techniques and libraries to provide engineers with the flexibility they need, without sacrificing performance.

7.2 Representative Flight Software TRN Algorithms

We have developed representative flight software implementations of TRN algorithms in the commonly used cFS ecosystem[22]. The implemented algorithms include in-flight template rendering and cross-correlation based matching for monocular images and direct altimetry measurements for active sensors (LIDAR and Altimeters). These are released to serve as examples of how FSW can be integrated into the validation pipeline tool.

8 Preliminary Technology Transfer Plan Summary

Each of the sections in this document contains information on how each set of maps is generated and the tools and methods used. Each section also includes a statement on technology transfer. As a summary, except for the tools described in Sections 3, 4, and possibly Section 2, the project plans to first publish a detailed description of the tools described in this document (either in conference or peer reviewed papers) and then work towards preparing the applicable software tools for release. We also plan to release a summary document, similar to this one, publicly which provides the locations of all released tools and datasets.

References

[1] Michael K. Barker, Erwan Mazarico, Gregory A. Neumann, David E. Smith, Maria T. Zuber, and James W. Head. Improved LOLA elevation maps for south pole landing sites: Error estimates and their impact on illumination conditions. *Planetary and Space Science*, 203:105119, 2021.

[2] Michael K. Barker, Erwan Mazarico, Gregory A. Neumann, David E. Smith, Maria T. Zuber, James W. Head, and Xiaoli Sun. A New View of the Lunar South Pole from the Lunar Orbiter Laser Altimeter (LOLA). *The Planetary Science Journal*, 4:183, 9 2023.

[3] M.K. Barker, E. Mazarico, G.A. Neumann, M.T. Zuber, J. Haruyama, and D.E. Smith. A new lunar digital elevation model from the Lunar Orbiter Laser Altimeter and SELENE Terrain Camera. *Icarus*, 273:346–355, 2016.

[4] GDAL/OGR contributors (2020). GDAL/OGR Geospatial Data Abstraction Software Library, Open. Source Geospatial Foundation http://www.gdal.org.

[5] Jason R. et al. Laura. ISIS 6.0.0 Public Release. Zenodo, https://doi.org/10.5281/zenodo.5347823, 2021.

[6] Ross. A. Beyer, Oleg Alexandrov, and Scott McMichael. The Ames Stereo Pipeline: NASA's open source software for deriving and processing terrain data. *Earth and Space Science*, 5:537–548, 2018.

[7] Oleg Alexandrov and Ross. A. Beyer. Multi-view shape-from-shading for planetary images with challenging illumination. *Earth and Space Science*, in revision, 2018.

[8] Bo Li, Zongcheng Ling, Jiang Zhang, and Jian Chen. Rock size-frequency distributions analysis at lunar landing sites based on remote sensing and in-situ imagery. *Planetary and Space Science*, 146:30–39, 2017.

[9] N. E. Demidov and A. T. Basilevsky. Height-to-diameter ratios of moon rocks from analysis of Lunokhod-1 and -2 and Apollo 11–17 panoramas and LROC NAC images. *Solar System Research*, 48(5):324–329, 2014.

[10] R. L. Heacock, G. P. Kuiper, E. M. Shoemaker, H. C. Urey, and E. A. Whitaker. Ranger VIII and IX Part II. Experimenters' Analyses and Interpretations. Technical report, NASA JPL, 1966.

[11] Caleb I. Fassett and Bradley J. Thomson. Crater degradation on the lunar maria: Topographic diffusion and the rate of erosion on the Moon. *Journal of Geophysical Research: Planets*, 119(10):2255–2271, 2014.

[12] Caleb I. Fassett, Ross A. Beyer, Ariel N. Deutsch, Masatoshi Hirabayashi, CJ Leight, Prasun Mahanti, Cole A. Nypaver, Bradley J. Thomson, and David A. Minton. Topographic Diffusion Revisited: Small Crater Lifetime on the Moon and Implications for Volatile Exploration. *Journal of Geophysical Research: Planets*, 127(12):e2022JE007510, 2022. e2022JE007510 2022JE007510.

[13] Julie D. Stopar, Mark S. Robinson, Olivier S. Barnouin, Alfred S. McEwen, Emerson J. Speyerer, Megan R. Henriksen, and Sarah S. Sutton. Relative depths of simple craters and the nature of the lunar regolith. *Icarus*, 298:34–48, 2017. Lunar Reconnaissance Orbiter - Part III.

[14] Yueyang Li, Wenzhe Fa, and Bojun Jia. Morphological Characterization of Decimeter- to Hectometer-Scale Impact Craters at the Chang'E-3/4/5 Landing Sites. *Journal of Geophysical Research: Planets*, 128(4):e2022JE007703, 2023. e2022JE007703 2022JE007703.

[15] Barry C Roberts. Cross-Program Design Specification for Natural Environments (DSNE) Revision G. Technical report, NASA, December 2019.

[16] G. Neukum, B. A. Ivanov, and W. K. Hartmann. Cratering Records in the Inner Solar System in Relation to the Lunar Reference System. *Space Science Reviews*, 96(1):55–86, 2001.

[17] E. Grün, H.A. Zook, H. Fechtig, and R.H. Giese. Collisional balance of the meteoritic complex. *Icarus*, 62(2):244–272, 1985.

[18] NASA. Astromaterials 3D: Apollo Lunar Samples. Apollo Rock Library, https://ares.jsc.nasa.gov/astromaterials3d/apollo-lunar.htm, 2024. Astromaterials 3D, NASA Johnson Space Center.

[19] Andrew J. Liounis, Christopher Gnam, Jason Swenson, Kenneth Getzandanner, Jeffrey Small, and Joshua Lyzhoft. The Goddard Image Analysis and Navigation Tool, 1 2022. https://github.com/nasa/giant.

[20] NASA Jet Propulsion Laboratory. MontePy: Python Tools for Monte. https://montepy.jpl.nasa.gov/, 2024. NASA Jet Propulsion Laboratory, California Institute of Technology.

[21] Anne C. Long, David Gaylor, and Nathan Stacey. Goddard Enhanced Onboard Navigation System (GEONS) Mathematical Specifications. https://ntrs.nasa.gov/citations/20240004259.

[22] National Aeronautics and Space Administration. Core Flight System (cFS), 2023. NASA Goddard Space Flight Center.

Acronyms

GCD Game Changing Development Program
DEM Digital Elevation Model
TRN Terrain Relative Navigation
HDA Hazard Detection and Avoidance
GEONS Goddard Enhanced Onboard Navigation System
GIANT Goddard Image Analysis and Navigation Tool
OD Orbit determination
ESM Entry Systems Modelling
FSW Flight Software
cFS core Flight System
SfS Shape from Shading
ASP Ames Stereo Pipeline
LROC Lunar Reconnaissance Orbiter Camera
SLT Synthetic Lunar Terrains
API Application Programming Interface
LuNaMaps Lunar Navigation Maps
PDS Planetary Data Sciences
pix pixel